# 68Ga-Labeled Gold Glyconanoparticles for Exploring Blood–Brain Barrier Permeability: Preparation, Biodistribution Studies, and Improved Brain Uptake via Neuropeptide Conjugation

Jens Frigell,[†] Isabel García,[†,‡] Vanessa Gómez-Vallejo,[§] Jordi Llop,[§] and Soledad Penadés*[,†,‡]

[†]Laboratory of GlycoNanotechnology, Biofunctional Nanomaterials Unit, CIC biomaGUNE, [‡]CIBER-BBN, and [§]Radiochemistry Department, Molecular Imaging Unit, CIC biomaGUNE, Parque Tecnológico, Paseo Miramón 182, 20009 San Sebastian, Spain

Ⓢ Supporting Information

ABSTRACT: New tools and techniques to improve brain visualization and assess drug permeability across the blood–brain barrier (BBB) are critically needed. Positron emission tomography (PET) is a highly sensitive, noninvasive technique that allows the evaluation of the BBB permeability under normal and disease-state conditions. In this work, we have developed the synthesis of novel water-soluble and biocompatible glucose-coated gold nanoparticles (GNPs) carrying BBB-permeable neuropeptides and a chelator of the positron emitter ^{68}Ga as a PET reporter for in vivo tracking biodistribution. The small GNPs (2 nm) are stabilized and solubilized by a glucose conjugate. A NOTA ligand is the chelating agent for the ^{68}Ga, and two related opioid peptides are used as targeting ligands for improving BBB crossing. The radioactive labeling of the GNPs is completed in 30 min at 70 °C followed by purification via centrifugal filtration. As a proof of principle, a biodistribution study in rats is performed for the different ^{68}Ga-GNPs. The accumulation of radioactivity in different organs after intravenous administration is measured by whole body PET imaging and gamma counter measurements of selected organs. The biodistribution of the ^{68}Ga-GNPs varies depending on the ligands, as GNPs with the same gold core size show different distribution profiles. One of the targeted ^{68}Ga-GNPs improves BBB crossing near 3-fold (0.020 ± 0.0050% ID/g) compared to nontargeted GNPs (0.0073 ± 0.0024% ID/g) as measured by dissection and tissue counting.
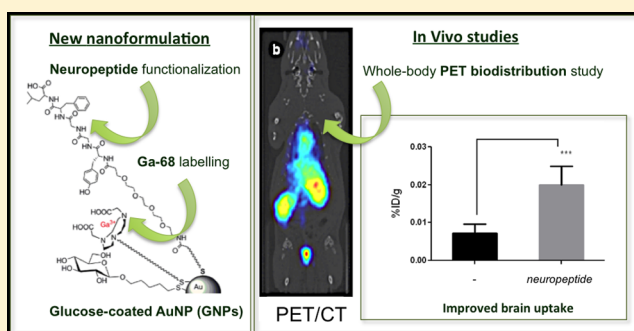
INTRODUCTION

Neurological diseases include a range of disorders that affect a large percentage of the world's population. Even though the biological basis underlying many of such disorders is often known, the therapeutic efficacy is limited due to the selectivity of the blood–brain barrier (BBB).[1,2] The BBB consists of endothelial cells separated by tight junctions, and it plays an effective role in protecting the brain from harmful substances and microorganisms. At the same time, the BBB hampers the systemic delivery of therapeutic agents from the blood into the brain.[3,4] Drugs should be small (molecular weight below 400 Da) and lipophilic to traverse the BBB, and they should not be a substrate of the efflux system such as P-glycoproteins. In practice, few drugs meet these specifications, and most therapeutic agents targeting the central nervous system (CNS) must cross the BBB through interaction with specific transporters or receptors expressed at the luminal side of the endothelial cells.[5] Additionally, poor stability in vivo of drugs such as peptides and nucleosides also limits systemic drug administration targeting the CNS.

Engineered biomaterials and polymeric nanoparticles have arisen as promising alternatives to promote brain protection and repair and to improve the delivery of therapeutic agents into the CNS.[6–9] Nanoparticles (NPs) have the capacity to be loaded with therapeutic agents and deliver cargo selectively to the site of action, increasing the therapeutic efficacy and reducing undesired side effects. Additionally, compared to molecular scale agents, NPs have prolonged circulation times and enable multivalent interactions. Numerous reports exist on molecules and macromolecules that have been anchored to liposomes, dendrimers, and polymeric nanoparticles in order to interact with transporters or receptors of endothelial cells and thus improve BBB penetration. Examples include proteins (lactoferrin),[10] antibodies (apolipoprotein E[11] or antitransferrin[12]), peptides (TAT,[13] bacteriophage Clone 12-2 peptide,[14] RVG-9R peptide,[15] angiopeptides[16]), and bioadhesive surfactants such as polysorbate 80.[17] However, there is still a need for tools with efficient BBB permeability and enhanced targeting properties.

Many metallic nanoparticles have been designed to be biocompatible and furthermore to be used as contrast agents for in vivo imaging by different techniques. There are also reports on NPs that have been functionalized with targeting ligands in order to facilitate BBB crossing by selective or preferential interaction with receptors or transporters.[16,18–23]
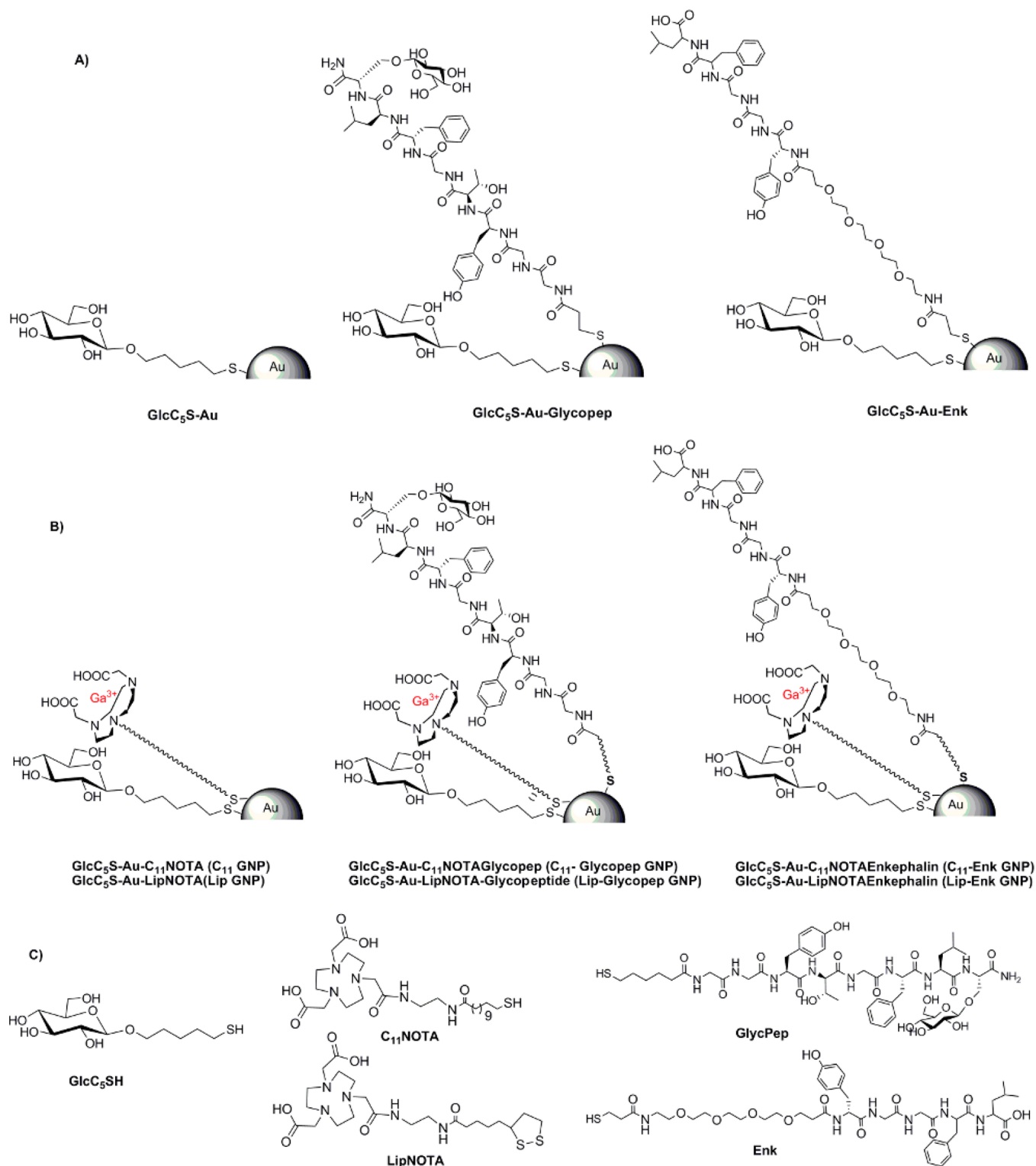
Figure 1. (A) Control and precursor glyconanoparticles (GNPs) employed in the preparation of the different [68]Ga- labeled GNPs. (B) Prepared nontargeted and targeted ^{68}Ga-GNPs for in vivo studies. (C) Ligands used for the synthesis of ^{68}Ga-GNPs.

Among metallic nanoparticles, gold nanoclusters are an excellent platform to combine therapeutic and diagnostic agents for noninvasive visualization of drug delivery.[24]

Our experience in the design and preparation of biocompatible sugar-coated gold nanoparticles (glyconanoparticles, GNPs) for a variety of biomedical applications[25−27] prompted us to address the preparation of gold GNPs able to reach an intact brain. GNP methodology allows the incorporation of multiple ligands in a controlled fashion.[26] The hydrophilicity of sugars confers biocompatibility[27] and resistance to protein adhesion to nanomaterials.[28] We reasoned that decorating GNPs with molecules that can access the brain (i.e., glucose, neuropeptides) in combination with a gallium-68 (^{68}Ga) chelator might result in highly sensitive PET probes as a tool

Table 1. Properties and Average Chemical Composition of GNPs[a]

GNPs	TEM d(nm)	ligands per GNP	glucoseC$_5$SH per GNP	peptides per GNP[b]	NOTA per GNP	MW[c] (kDa)
GlcC$_5$S−Au	1.8 ± 0.2	87	87			64
LipGNP	2.2 ± 0.2	80	67		13[d]	87
C$_{11}$GNP	2.4 ± 0.2	130	110		20[d]	132
Lip-EnkGNP	2.1 ± 0.2	80	59[e]	13	8[e]	94
C$_{11}$-EnkGNP	2.7 ± 0.3	135[f]	106	10	19	162
Lip-Glycopep GNP	2.2 ± 0.2	80	60[e]	6	14[e]	92
C$_{11}$-Glycopep GNP	3.2 ± 0.3	221[f]	174	15	32	329

[a]All GNPs are coated with and stabilized by GlcC$_5$SH ligand. [b]The amount of peptide on the GNPs was assessed by quantitative ^{1}H NMR with the internal standard TSP and integration of the aromatic proton region of the spectrum. [c]Calculated from the number of Au atoms as derived from the TEM diameter plus the number of ligands and their molecular weight.[63] [d]Determined by elemental analysis. [e]Derived from known ratio of GlcC$_5$SH and NOTA ligand in the precursor GNP and assuming that the total amount of ligands does not change. [f]The total ligands per GNPs were estimated based on the average gold diameter and according to the literature.[63]

to visualize biodistribution and evaluate brain uptake in small animals. To date, different in vitro and in vivo methods have been applied to assess BBB permeation of drugs. However, noninvasive molecular imaging techniques such as positron emission tomography (PET), combined PET/computed tomography (PET/CT), and magnetic resonance imaging (MRI) provide the most accurate information regarding in vivo biodistribution and brain uptake in animals with uncompromised BBB.[29,30]

In this work, we report the preparation of nontargeted and targeted glucose/^{68}Ga-coated gold nanoparticles (^{68}Ga-GNPs) as novel nanosystems for the assessment of in vivo biodistribution and BBB permeation. Nontargeted GNPs incorporate a glucose conjugate (GlcC$_5$S) and a thiol-ending derivative of a cyclic ^{68}Ga chelator. To convert nontargeted GNPs into targeted GNPs in order to achieve BBB crossing, two neuropeptide derivatives were selected, either the pentapeptide Tyr-Gly-Gly-Phe-Leu (Enk) or the glycosylated peptide Gly-Gly-Tyr-Thr-Gly-Phe-Leu-Ser-O-β-glucoside (Glycopep). Small neuropeptide derivatives from the enkephalin family ([H$_2$N-Tyr-Gly-Gly-Phe-Leu(Met)-COOH]) and related glycopeptides have frequently been used as suitable vectors for BBB passage.[31−34] However, their low stability and poor bioavailability in vivo due to enzymatic degradation have limited their efficacy. Different strategies to achieve improved stability and bioavailability of the peptides, including glycosylation, lipidation, and pegylation among others, have been reported.[33] Here, we propose that the incorporation of small, modified neuropeptides onto the GNP surface improves the peptide stability and enhances the capability to reach and bind to their natural targets. After the GNPs were labeled, in vivo biodistribution PET studies in rodents were performed in combination with dissection and tissue counting experiments. A significant improvement of BBB penetration for one of the targeted GNPs was observed.

■ RESULTS AND DISCUSSION

Synthesis of Glyconanoparticles and Incorporation of the Chelating Agent. Our ^{68}Ga-labeled glyconanoparticles (^{68}Ga-GNPs) are based on 2 nm gold nanoparticles coated with a glucose conjugate (GlcC$_5$S). Among all radionuclides, gallium-68 (^{68}Ga) was selected because, contrary to other positron emitters that have to be produced in cyclotrons, ^{68}Ga can be obtained from a ^{68}Ge−^{68}Ga generator and can be eluted on a daily basis.[35] In addition, it has 89% positron branching and low photon emission. As far as we know, only a few examples of ^{68}Ga-labeled polymeric NPs[36−39] exist, and only

one example of ^{68}Ga-labeled magnetic NPs has been reported to date.[19]

Two types of ^{68}Ga-GNPs (nontargeted and targeted GNPs) were prepared (Figure 1). The nontargeted GNPs, GlcC$_5$S-Au-C$_{11}$NOTA (**C$_{11}$GNP**) and GlcC$_5$S-Au-LipNOTA (**LipGNP**) incorporate glucose and the cyclic chelator 1,4,7-triazacyclono-nane-1,4,7-triacetic acid (NOTA), which forms a stable complex with Ga(III) (log K = 30.98).[40] The targeted GNPs, GlcC$_5$S-Au-C$_{11}$NOTAEnkephalin (**C$_{11}$-EnkGNP**), GlcC$_5$S-Au-LipNOTAEnkephalin (**Lip-EnkGNP**), GlcC$_5$S-Au-C$_{11}$NOTAGlycopep (**C$_{11}$GlycopepGNP**), and GlcC$_5$S-Au-LipNOTAGlycopep (**Lip-GlycopepGNP**) incorporate two peptides, the pentapeptide Tyr-Gly-Gly-Phe-Leu (Enk) or the glycosylated peptide Gly-Gly-Tyr-Thr-Gly-Phe-Leu-Ser-O-β-glucoside (Glycopep) (Figure 1B). Control and precursor GNPs (Figure 1A) bearing either glucose (GlcC$_5$S-Au), glucose and the Enk peptide (GlcC$_5$S-Au-Enk) or glucose and the glycosylated peptide (GlcC$_5$S-Au-Glycopep) were also prepared following a one-pot protocol. All prepared GNPs and the thiol-ending ligands used in their preparation are shown in Figure 1.

For the preparation of the nontargeted GNPs, the glycoconjugate 5-mercaptopentyl β-D-glucopyranoside (GlcC$_5$S)[41,42] and two different NOTA conjugates, LipNOTA and C$_{11}$NOTA (Figure 1C), were synthesized. The NOTA was functionalized with linkers containing a thiol-ending group for attaching the chelator to the gold surface. Two linkers, an 11-carbon atom aliphatic chain (C$_{11}$) and a lipoic acid (Lip), were selected for the preparation of the C$_{11}$NOTA and LipNOTA conjugates (Figure 1C and Scheme S1, Supporting Information), in order to investigate their effect on the in vivo ^{68}Ga-GNPs biodistribution pattern. The **C$_{11}$GNP** and **LipGNP** (Figure 1B) were prepared by in situ reduction (one-pot reaction) of HAuCl$_4$ with NaBH$_4$ in the presence of an excess of thiol-ending compounds following a previously described protocol.[42] The GNPs were purified by centrifugal filtration and dialysis and characterized by ^{1}H NMR, IR, UV−vis, TEM, and elemental analysis (see the Supporting Information). The ratio between the glucoside and the NOTA conjugates on the GNPs was determined by elemental analysis of the GNP, since the NOTA conjugate contains nitrogen atoms whereas the glucoside does not. An average percentage of 84/15 of glucose to NOTA per GNP was determined on the basis of the number of ligands (Table 1). The ratio of glucose/NOTA conjugates was also confirmed by comparing the ^{1}H NMR spectra of the conjugates mixture before and after formation of the GNPs.

Preparation of GNPs Incorporating the Peptides. In order to prepare targeted GNPs and to test the capacity of the small-sized (2 nm) GNPs to penetrate the BBB in rodents, the Leu-enkephalin (Tyr-Gly-Gly-Phe-Leu, Enk) peptide, modified with a thiolated PEG linker, and the glycosylated peptide, Gly-Gly-Tyr-Thr-Gly-Phe-Leu-Ser-O-β-glucoside (Glycopep), modified with a thiopentyl chain, were prepared (Figure 1C and Figure S1, Supporting Information). Similar peptides have been shown to be able to cross the BBB.[43,44] Although Leu-enkephalin is known to rapidly undergo enzymatic cleavage in vivo,[45,46] improved stability toward enzymatic hydrolysis can be expected because of the attachment onto the GNPs surface. Enhanced resistance toward *E. coli* β-galactosidase hydrolysis was observed for lactose on GNPs compared to the free disaccharide.[47]

The targeted ^{68}Ga-GNPs, **C$_{11}$-GlycopepGNP**, **Lip-Glyco-pepGNP**, **C$_{11}$-EnkGNP**, and **Lip-EnkGNP** (Figure 1B), capped with the peptides were prepared by ligand place exchange reaction (LPE).[48] This methodology allows modification of the organic shell of previously prepared GNPs by exchange with other thiolated ligands. **Lip-Glycopep GNP** and **Lip-EnkGNP** were prepared by mixing an aqueous solution of GlcC$_5$S-Au-LipNOTA GNPs with an aqueous solution of the respective peptide derivative (0.3−1.2 equiv with respect to the glucose on the GNP) at 25 °C for 48 h and 180 rpm. In the case of the **C$_{11}$-GlycopepGNP** and the **C$_{11}$-EnkGNP**, the LPE was performed starting from GlcC$_5$S-Au-Glycopep GNP or GlcC$_5$S-Au-Enk GNP (Figure 1A) and subsequent addition of an excess of the C$_{11}$−NOTA conjugate (2−10 equiv with respect to glucose on the GNP). The functionalized GNPs were purified as before and characterized by TEM, UV−vis, IR, and ^{1}H NMR (see the Supporting Information). The amount of peptide on the GNPs was assessed by quantitative ^{1}H NMR by integration of the aromatic proton region of the spectrum, which only contained signals from the peptide, and using trimethylsilyl propanoic acid (TSP) as internal standard (Figure S2, Supporting Information). Alternatively, when insertion of the peptides was performed following the one-pot protocol, peptide load was determined by comparing the ligand mixture before and after GNPs production using ^{1}H NMR. Table 1 summarizes the average core size diameter, number of ligands, organic shell composition, and calculated molecular weights for the prepared GNPs.

Incorporation of ^{68}Ga to Radiolabel the Nanoparticles. Incorporation of the radionuclide ^{68}Ga was performed in the very last step. The labeling efficiency was investigated using different reaction conditions (temperature, stoichiometry, and reaction time). As previously reported, Ga(III) chelation worked best at pH ca. 3.5.[49] Typically, 200 μg of GNP were reacted with 37−74 MBq of ^{68}Ga contained in 0.4 mL of 0.6 N aqueous HCl solution as obtained from the ^{68}Ge−^{68}Ga generator (pH of the reaction was adjusted with HEPES and NaOH). ^{68}Ga incorporation efficiencies ranging from 85% to 94% were obtained within 30 min at 70 °C for all GNPs (Figure S3, Supporting Information). Shorter reaction times at 70 °C did not complete the chelation of Ga-68 as seen by radio-TLC (Figure S4, Supporting Information). When the labeling was carried out at 30 °C, lower incorporation efficiencies were achieved: only 23% of the activity was chelated to the GNP and 77% was found in the washings (Figure S5, Supporting Information). Increasing the amount of radioactivity at the expense of lowering the concentration of GNP did not enhance the overall radiochemical yield. After the

reaction, nonchelated ^{68}Ga was removed by centrifugal filtration and repeated centrifugal washings with PBS buffer (pH 7.4) until no radioactivity was detected in the washings. The overall preparation, including washing, could be performed in less than 60 min. The high number of NOTA molecules (8−32 per GNP, Table 1) ensured ^{68}Ga incorporation to obtain specific activity values higher than 0.11 MBq/μg GNP. Such high specific activities are essential in order to decrease the administered dose in the in vivo investigations, which in our case was 150−200 μg GNP/180−250 g body weight (3.7−14.8 MBq), thus minimizing potential toxicological effects. In addition, in vitro stability test (2 h, at 37 °C in saline buffer) showed a very slow release of ^{68}Ga from GNPs (after 2 h of incubation, radiochemical purity >85%), again pronouncing the suitability of ^{68}Ga-labeled GNPs for in vivo PET studies.

Finally, control labeling experiments (70 °C, pH 3.5, 30 min) were carried out with GNPs containing only glucose (GlcC$_5$S−Au) or glucose and the peptides (GlcC$_5$S-Au-Enk or GlcC$_5$S-Au-Glycopep, Figure 1A) in order to test that ^{68}Ga is only attached to NOTA and that no radiolabeling of the GNPs occurred due to unspecific complexation of ^{68}Ga ion to glucose and/or peptides. After labeling, the free ^{68}Ga was removed from the GNPs by centrifugal filtration and washing. Gamma counter analysis of the washings and the GNPs confirmed the lack of radioactive labeling of glucose bearing GNPs and a very low ^{68}Ga incorporation in the peptide-bearing GNPs. This result clearly indicates that effective radiolabeling is only achieved via the formation of ^{68}Ga-NOTA complex (Figures S6 and S7, Supporting Information).

In Vivo Studies with ^{68}Ga-Labeled Gold Nanoparticles. It is well-known that systemically administered nanoparticles accumulate in different organs depending mainly on particle size. As a general rule, large particles are trapped in the smallest capillaries of the lungs or engulfed by phagocytic cells in the organs of the reticulo-endothelial system (RES) such as the liver, the spleen, and the lungs, while smaller particles reach various organs by crossing the tight endothelial junctions and are rapidly excreted through the kidneys.[50−52] However, the clearance from the bloodstream and the accumulation in different organs depends also on other intrinsic properties such as surface decoration and surface charge, with opsonization also playing an important role in macrophage recognition.[53] Biodistribution and accumulation of gold nanoparticles in different organs depend on the size core,[54] but also on the coating and administration route.[55] In the case of ^{68}Ga-GNPs reported here, all particles have similar core sizes (2−3 nm) as determined by TEM (micrographs in the Supporting Information). Any differences in biodistribution should be attributed to the difference in the coating ligands and not to the variability of the gold core sizes.

The biodistribution of ^{68}Ga-GNPs with and without targeting peptides was investigated in 7−8 week old (180−250 g body weight) Sprague−Dawley rats. Typically, labeled GNPs (0.75−1.0 μg/μL) were injected (200 μL, 3.7−14.8 MBq, 100−400 μCi) via one of the lateral tail veins. The dynamic evolution of the GNP accumulation in different organs was assessed using PET/CT during 4 h after intravenous (iv) administration. Images were acquired in four bed positions in order to cover the whole body of the animal. Averaged time−activity curves (TACs) for all GNPs (n = 3 animals per nanoparticle) were obtained. A steady-state-like behavior was reached for the majority of the organs and GNPs after 1 h. At the end of the scans, the animals were sacrificed without recovering from
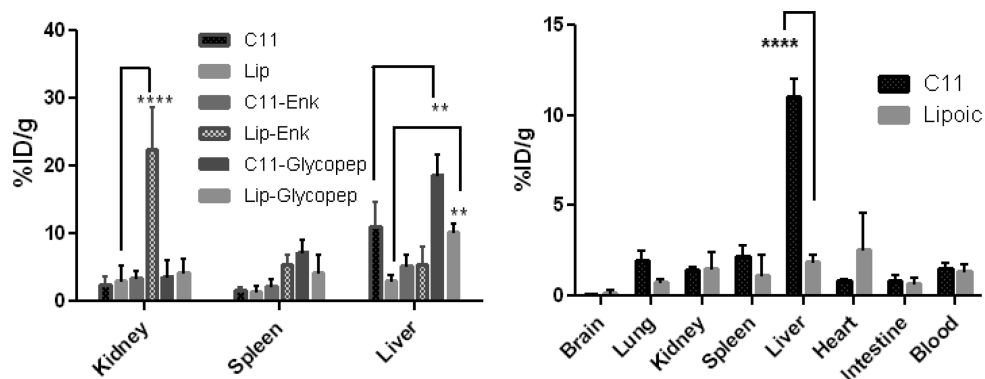
Figure 2. (Left) Biodistribution data of selected organs in Sprague−Dawley rats at time of harvesting. The uptake of different GNPs is represented as percentage of radioactivity per injected dose, per unit mass of organs, and per animal weight. (Right) Comparison of accumulation of C_{11}GNP and LipGNP in different organs. Each bar represents the mean ± SEM of 3 rats. ****$P < 0.0001$Lip vs Lip-Enk in kidney uptake, **$P < 0.01C_{11}$ and Lip vs C11-Glycopep and Lip-Glycopep; ****$P < 0.0001C_{11}$ vs Lip in liver uptake.
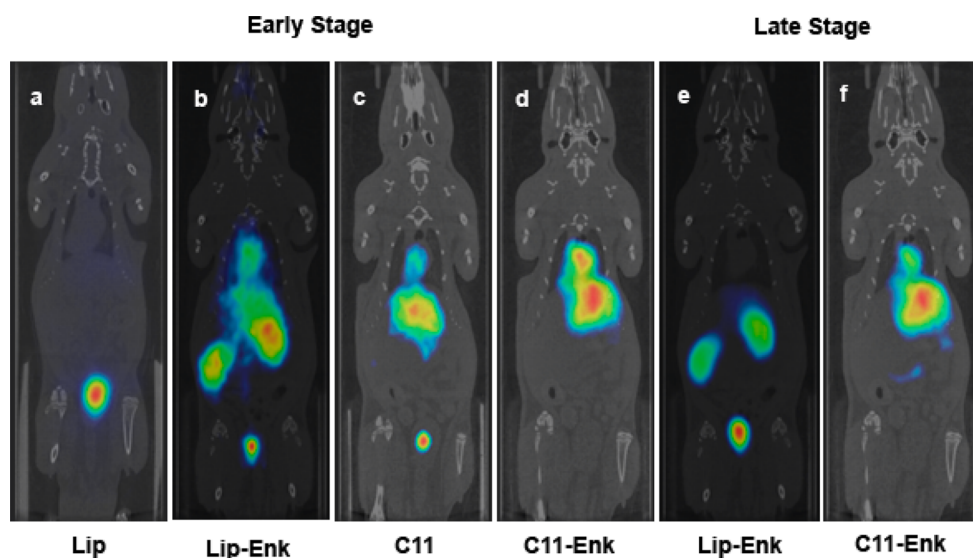

Figure 3. Co-registered coronal PET/CT images of the ^{68}Ga-GNPs: LipGNP (a), Lip-EnkGNP (b), C_{11}GNP (c), and C_{11}-EnkGNP (d) at early stage (0−10 min) and Lip-EnkGNP (e) and C_{11}-EnkGNP (f) at late stage (60−80 min) after iv injection.

anesthesia, the organs were harvested, and the amount of radioactivity was determined using a gamma counter (dissection and tissue counting). The vast majority of the GNPs were excreted in urine, which was not collected during the PET scan. After the scan, urine still in the bladder was collected and measured for radioactivity in the gamma counter. Figure 2 (left) shows the accumulation of different labeled GNPs in selected organs at the time of sacrifice (4 h post injection) as determined by organ removal and gamma counting. Results showed a major accumulation in liver, spleen, and kidneys; however, a significant influence of the ligands on the biodistribution pattern was observed. The presence of the peptide influenced the biodistribution of the ^{68}Ga-GNPs (Lip-GNP vs LipEnk-GNP in kidney, Figure 2 left). The glycopeptide seems to contribute to an increased accumulation in the liver, especially for those GNPs bearing the C_{11}NOTA ligand (C_{11}-GlycopepGNP). A comparison of liver accumulation of the nontargeted C_{11}GNP and LipGNP confirms that the nature of the linker in the NOTA conjugates has a significant impact on the biodistribution pattern (Figure 2 right). GNPs with a longer aliphatic chain (C_{11}) accumulate to a greater extent in the liver in comparison to GNPs bearing the

NOTA conjugate with shorter linker (Lip). A similar effect was previously reported by Sá et al. for non-nanoparticulated Ga(III) chelates,[56] suggesting that the organic molecules bound to very small nanoclusters may present similar physicochemical and biological properties to those shown when they are free.

The in vivo images showed similar trends with respect to the gamma counter evaluation. Reconstructed PET/CT images of rats injected with C_{11}GNP, LipGNP, and their respective enkephalin targeted GNPs (C_{11}-EnkGNP and Lip-EnkGNP) at early and late stages after administration also showed a different behavior depending on the ligands (Figure 3). At the early stage, Lip-GNP accumulated quickly in the bladder (∼70−90% ID/cm^3 after 10 min) (Figure 3a), while Lip-EnkGNP showed significant uptake in the kidneys (Figure 3b). However, ^{68}Ga-GNPs conjugated to C_{11}NOTA with or without enkephalin, rapidly accumulated in liver (Figures 3c and 3d). At a late stage of the scan (60−80 min), the C_{11}-EnkGNP was still accumulated in the liver (Figure 3f), whereas the Lip-EnkGNP was almost completely excreted (Figure 3e). The biodistribution of Lip-EnkGNP followed a similar pattern to that shown by the nontargeted LipGNP, only with a slightly higher accumulation in the kidneys (∼20−30% ID/cm^3 after 10 min)
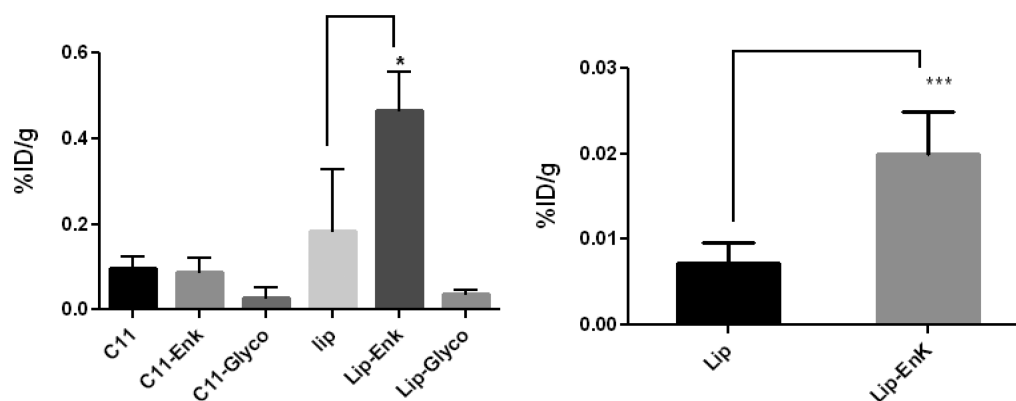
Figure 4. Brain uptake obtained after administration of the different GNPs using dissection and counting without (left) and with blood perfusion (right). Results are expressed as percentage of injected dose per gram of tissue. Each bar represents mean ± SEM of 3 (left) or 5 (right) animals. Significantly different from no targeted GNP: $*p < 0.05$, $***p < 0.001$.

and a delayed peak in bladder accumulation (20 min after injection) (Figure 3a and 3b). Rapid renal clearance is expected for small nanoparticles and is consistent with values reported in the literature, but the different biodistribution profile between the 2 nm sized **Lip-EnkGNP** and **C$_{11}$-EnkGNP** should be attributed to the linker's nature. The presence of GNPs in other organs such as spleen, heart, and intestine was also detected.

Even though the vast majority of intravenously injected gold nanoparticles accumulate in the liver and the spleen,[57,58] the conjugation to sugar molecules can greatly change the pharmacokinetic behavior by reducing the nonspecific adsorption of plasma proteins and preventing uptake by the RES similarly as polyethylene glycol does.[59] In this respect, glucose grafting density on the **Lip-GNP** might be able to decrease opsonization leading to low liver accumulation. This is especially relevant since liver accumulation and subsequent hepatic toxicity have previously prevented the application of potentially effective drug delivery systems.

Gamma counter measurements performed on harvested brains showed almost 2.5-fold higher uptake values in the brain of animals injected with **Lip-EnkGNP** compared to those receiving the nontargeted nanoparticles, **Lip-GNP** (Figure 4, left). PET/CT image quantification also validated the higher brain uptake for animals injected with **Lip-EnkGNP**. For the quantification, frames at $t > 54$ min after injection were averaged and uptake values expressed as % of injected dose per body weight (%ID/g) (Figure S8, Supporting Information). These results might have been influenced to some extent by the presence of ^{68}Ga-GNPs in blood. Therefore, building on these encouraging results, the experiments were repeated with **Lip-EnkGNP** and **LipGNP**, but the animals ($n = 5$) were perfused before organ harvesting using physiologic saline solution. As seen in Figure 4 (right), the targeted GNPs have a 2.7-fold higher accumulation in brain compared to nontargeted particles ($p < 0.001$). To further validate these results, the gold content in the brain was determined by ICP-MS. The result also confirms a higher accumulation of gold in extracted brains of rats injected with **Lip-EnkGNP** (0.07 ppm) when compared to animals injected with the nontargeted **LipGNP** where gold was not detected (<0.05 ppm, detection limit of the technique).

An evaluation of the brain permeability obtained with the novel gold ^{68}Ga-GNPs in comparison with other targeted nanoparticles is not straightforward. Most of the reported NPs designed to target the brain are liposomes or polymeric NPs. They have so far reached the brain ranging from 0.01% to 0.5%

of the ID when vascular rectification was applied.[28,60−62] In the case of the gold **Lip-EnkGNP** (~13 peptides/GNP), a ~0.025% of the injected dose accumulated in the brain after iv injection of a maximal dose of 200 μg GNP/rat (Figure 4, right). This result is similar to that obtained (0.024%) with high-loading amphipathic peptide gold nanoparticles (400 peptides/NP) after intraperitoneal injection.[20] Notably, in our experiments as little as 28.8 μg of peptide (injected dose = 0.12 mg peptide/kg) was injected. This value is 2 orders of magnitude lower than the doses previously utilized with enkephalin peptide analogues (30−122 mg/kg) to achieve an analgesic effect.[31,32] Despite the low peptide dose injected, the accumulation of the targeted GNPs in the brain was almost 3-fold to that of nontargeted GNPs. The improved bioavailability of the peptide is probably a result of an improved stability after conjugation to the nanoplatform. Preliminary in vitro results showed an enhanced stability for the peptide conjugated to the GNP compared to the free peptide when both were subjected to an endogenous peptidase under the same experimental conditions (data not shown).

The use of gold glyconanoparticles as carrier for BBB-permeable molecules is a promising field, due to almost endless possibilities of chemical functionalization and formulation of the GNPs. The introduction of molecular imaging reporters (PET in this case) expands their potential for in vivo imaging of brains with uncompromised BBB. In addition, the high molecular weight of the gold GNPs (50−300 kDa) allows a straightforward separation of the radiolabeled GNPs from free radioisotopes and small ligands and a convenient purification via centrifugal filtration rather than HPLC.

■ CONCLUSION

We have prepared and labeled novel targeted and nontargeted GNPs (^{68}Ga-GNPs) based on 2 nm sized gold glyconano-particles carrying the positron emitter ^{68}Ga for in vivo PET imaging. The nontargeted GNPs are coated with glucose, the brain's principal nutrient, and a NOTA derivative as gallium chelator. Two related neuropeptides were conjugated to the previous GNPs as targeting ligands for improving brain uptake. Depending on the nature of the ligands attached to the gold surface, a different biodistribution profile was observed. We have shown that targeted GNPs bearing a Leu-enkephalin peptide (Enk) improve brain accumulation (0.020 ± 0.0050% ID/g) nearly 3-fold compared to nontargeted GNPs (0.0073 ± 0.0024%ID/g). To our knowledge, this is the first report of

^{68}Ga-labeled gold nanoparticles that take advantage of the remarkable chemical versatility of gold nanoparticles as a scaffold for the attachment of a diversity of molecules in a controlled way. The novel radioactive ^{68}Ga-GNPs have enabled the quantification of BBB permeability in rodents with intact brains. The results here obtained also indicate that manipulation of the molecules coating GNPs may result in GNPs with more favorable properties to cross the blood−brain barrier. Metal chelators others than NOTA can be easily introduced on the GNPs expanding significantly the utilization of PET as an ultrasensitive imaging technique for the pharmacokinetic evaluation of new chemical entities.

■ EXPERIMENTAL SECTION

Materials and Methods. All chemicals were purchased as reagent grade from Sigma-Aldrich and were used without further purification. NO2AtBu-N-(aminoethyl)ethanamide was purchased from CheM-atech (France). UV−vis spectra were measured on a Beckman Coulter DU 800 spectrometer. Infrared spectra (IR) were recorded from 4000 to 500 cm^{-1} with a JASCO FT/IR 410 model spectrometer: solids were pressed into a KBr plate. ^{1}H NMR and ^{13}C NMR spectra were recorded on a Bruker AVANCE (500 MHz) spectrometer. Mass spectra were carried out with an Esquire 6000 ESIIon Trap from Bruker Daltonics. High-resolution mass spectra (HR-MS) were obtained using the matrix-assisted laser desorption/ionization (MALDI) technique with a 4700 Proteomics Analyzer (Applied Biosystems) with MALDI-time-of-flight (TOF) configuration. TEM analysis was carried out in a Philips JEOL JEM-2100F working at 200 kV. The number of gold atoms of the GNPs was deduced from the core size mesasured in TEM and estimated according to a previous work.[63] House distilled water was further purified using a Milli-Q reagent grade water system (Millipore). ^{68}Ga (T$_{1/2}$ = 68 min, β^+ = 89%, EC = 11%) was obtained as ^{68}GaCl$_3$ from an iThemba ^{68}Ge/^{68}Ga generator system (IDB Holland bv, Netherlands) with a nominal ^{68}Ge activity of 740 MBq. The generator was eluted with 0.6 M HCl solution (6 mL) and the eluate was collected in five fractions (1.5, 0.5, 0.5, 0.5, 3 mL, respectively). Fractions 2−4 contained the highest ^{68}Ga concentration typically within the range of 74−111 MBq/0.5 mL and were used without further purification. Organ activity was measured in an automatic gamma counter (2470 Wizard, Perkin-Elmer). The glucose conjugate was prepared as previously described.[41] The synthesis and characterization of NOTA derivatives is described in the Supporting Information.

General Procedure for Direct Synthesis of Gold GNPs. A 0.025 M solution of HAuCl$_4$ (1 equiv) in Milli-Q water was added to a 0.012 M solution of thiolated ligand (3 equiv) in MeOH. If more than one type of ligand was used a combined amount of 3 equiv was used with respect to HAuCl$_4$. A freshly prepared 1 M solution of NaBH$_4$ was added in portions to the mixture, and immediately a black precipitate was formed. The reaction was left on a shaker board (200 rpm) for 2 h at room temperature after which the shaking was stopped and the precipitate was allowed to sediment. The supernatant was taken off using a pipet, and the nanoparticles were washed once with MeOH before they were dissolved in H$_2$O and purified by dialysis (MWCO = 10k) for 3 days, changing the water twice per day. The glyconanoparticles were characterized and then lyophilized and stored.

General Procedure for Preparation of Gold GNPs by Ligand Place Exchange Reaction (LPE). The GNP (1 equiv with respect to glucoside) was dissolved in Milli-Q water, the thiol-ending functionalized peptide or 1,4,7-triazacyclononane-1,4,7-triacetic acid (NOTA) derivative (1 equiv) was added, and the mixture was shaken (180 rpm) for 2 days at room temperature under Ar atmosphere. After this time, the nanoparticles were separated from the solution by centrifugal filtration (MWCO 10000, 10 min). The GNPs were then in a similar fashion washed three times with Milli-Q water and lyophilized.

General Procedure for the Synthesis of ^{68}Ga-Labeled GNPs. To a vial containing HEPES (42 mg, 0.176 mmol) was added 400 μL of ^{68}Ga (^{68}GaCl$_3$ in 0.6 N HCl, 2−3 mCi/0.5 mL), and the pH was adjusted to 3.5 with 10% aqueous NaOH solution (75 μL). From a 1 μg/μL solution of nanoparticles in ultrapure water (Type I water, ISO 3696), 100−200 μL were added to the reaction vial, and the temperature was raised to 70 °C and incubated for 30 min. The reaction mixture was filtered by centrifugation (30k, 13400 rpm) for 6 min. The nanoparticles were washed three times by centrifugal filtering (30k, 13400 rpm, 5 min) with HEPES (0.1 M, pH 7.1) and once with 0.9% saline solution. GNPs were then suspended in 0.9% saline, and the amount of radioactivity was counted in a gamma counter (2470 Wizard, Perkin-Elmer). Simultaneously, all fractions corresponding to successive washings were also measured. The incorporation yield was calculated as the ratio between the amount of radioactivity in the fraction containing the GNPs and the sum of all fractions corresponding to the washings.

Animal Experiments. Animals were cared for and handled in accordance with the Guidelines for Accommodation and Care of Animals (European Convention for the Protection of Vertebrate Animals Used for Experimental and Other Scientific Purposes). Internal guidelines and experimental procedures were approved by local authorities. Male, 7−8 weeks of age Sprague−Dawley rats (body mass 180−250 g) were used. Three animals per GNP were submitted to PET/CT studies followed by dissection and counting; 10 more animals were subjected to biodistribution studies using two different GNPs (n = 5 per GNP) via dissection and tissue counting with previous animal perfusion for complete blood removal.

Image Acquisition. PET studies were performed using an eXploreVista-CT small animal PET/CT system (General Electric Healthcare). For each GNP, three animals were submitted to whole body (WB) scans to assess the biodistribution pattern. In all cases, rats were anesthetized with a mixture of 3−4% isoflurane in O$_2$ for induction and reduced to 1−1.5% for maintenance in the camera by a nose cone to maintain regular breathing at a frequency of 60 ± 10 breaths/minute monitored by a pressure sensor (SA Instrument Inc., NY). Respiration and body temperature of the animals were monitored throughout the scan. The temperature, measured rectally, was maintained at 37 ± 1 °C using a water heating blanket (Homeothermic Blanket Control Unit, Bruker, Germany). For administration of the GNPs, the tail vein was catheterized with a 24-gauge catheter and 3.7−22.2 MBq of GNPs (150−300 μL, 100−200 μg) were injected in tandem with the start of the PET dynamic acquisition.

Dynamic images (20 frames: 4 × 2, 4 × 4, 3 × 10, 3 × 20, 3 × 30 min) were acquired in four bed positions in the 400−700 keV energy window, with a total acquisition time of 234 min; after each PET scan, CT acquisitions were also performed (140 μA intensity, 40 kV voltage), providing anatomical information as well as the attenuation map for the later image reconstruction. After finalizing the image acquisition, animals were sacrificed, and brain, lungs, kidneys, spleen, liver, heart, and intestine were quickly removed and measured in an automatic gamma counter (2470 Wizard, Perkin-Elmer). Blood samples (0.5 mL) were also taken and measured in the gamma counter.

Image Analysis. Dynamic acquisitions were reconstructed (random, scatter, decay and CT-based attenuation corrected) with filtered back projection (FBP) using a Ramp filter with a cut-off frequency of 1 Hz. PET images were analyzed using PMOD image analysis software (PMOD Technologies Ltd., Zürich, Switzerland). Volumes of interest (VOIs) were manually drawn (regions of interest (ROIs) in the Y-axis of the animal were added up to VOIs) for brain, liver, kidneys, lungs, heart, spleen, intestine, stomach, and bladder using the CT images as anatomical reference. VOIs were then transferred to the PET images, and the concentration of radioactivity was obtained for each organ and time frame as cps/cm^3. Values were transformed into real activity (Bq/cm^3). Finally, injected dose normalization was applied to data to obtain the percentage of injected dose per organ. After determination of the time activity curves, frames at t > 54 min (corresponding to the *plateau*) were averaged and the same quantification process was applied.

Dissection Method with Perfusion. Ten animals (5 per GNP) were submitted to biodistribution studies using perfusion and further

455

dx.doi.org/10.1021/ja411096m | J. Am. Chem. Soc. 2014, 136, 449−457

dissection and gamma counting. Rats were anesthetized with a mixture of 3−4% isoflurane in O_2 for induction and reduced to 1−1.5% for maintenance by a nose cone to maintain regular breathing at a frequency of 60 ± 10 breaths/minute monitored by a pressure sensor (SA Instrument Inc., NY). Respiration and body temperature of the animals were monitored throughout the study. The temperature, measured rectally, was maintained at 37 ± 1 °C using a water heating blanket (Homeothermic Blanket Control Unit; Bruker, Germany). For administration of the GNPs, the tail vein was catheterized with a 24-gauge catheter and 3.7−22.2 MBq of GNPs (150−300 µL, 100−200 µg) were injected. Two hundred forty minutes after administration, and without recovery from anesthesia, animals were perfused using saline solution. The brain was quickly removed, rinsed with deionized water, and measured in an automatic gamma counter (2470 Wizard, Perkin-Elmer).

ASSOCIATED CONTENT

Ⓢ Supporting Information

Supplemental figures, synthetic schemes, experimental procedures, characterization of all new compounds including GNPs, TEM images and size distribution histograms, and radio labeling as well as control experiments. This material is available free of charge via the Internet at http://pubs.acs.org.

AUTHOR INFORMATION

Corresponding Author

spenades@cicbiomagune.es

Notes

The authors declare no competing financial interest.

REFERENCES

(1) Pardridge, W. M. *J. Drug. Target* **2010**, *18* (3), 157−167.
(2) Nunes, A.; Al-Jamal, K. T.; Kostarelos, K. *J. Controlled Release* **2012**, *161*, 290−306.
(3) Miller, G. *Science* **2002**, *297*, 1116−1118.
(4) Praveen, B.; Alex, B.; Maiken, N. *Neurobiol. Dis.* **2004**, *16*, 1−13.
(5) Gabathuler, R. *Neurobiol. Dis.* **2010**, *37*, 48−57.
(6) Orive, G.; Anitua, E.; Pedraz, J. L.; Emerich, D. F. *Nat. Rev. Neurosci.* **2009**, *10*, 682−692.
(7) Wong, H. L.; Chattopadhyay, N.; Wu, X. Y.; Bendayan, R. *Adv. Drug Delivery Rev.* **2010**, *62*, 503−517.
(8) Malakoutikhah, M.; Teixidó, M.; Giralt, E. *Angew. Chem., Int. Ed.* **2011**, *50*, 7998−8014.
(9) Serwer, L. P.; James, C. D. *Adv. Drug Delivery Rev.* **2012**, *64*, 590−597.
(10) Huang, R.; Ke, W.; Liu, Y.; Jiang, C.; Pei, Y. *Biomaterials* **2008**, *29*, 238−246.
(11) Michaelis, K.; Hoffmann, M. M.; Dreis, S.; Herbert, E.; Alyautdin, R. N.; Michaelis, M.; Kreuter, J.; Langer, K. *J. Pharmacol. Exp. Ther.* **2006**, *317*, 1246−1253.
(12) Huwyler, J.; Wu, D.; Pardridge, W. M. *Proc. Natl. Acac. Sci. U.S.A.* **1996**, *93*, 14164−14169.
(13) Schwarze, S. R.; Ho, A.; Vocero-Akbani, A.; Dowdy, S. F. *Science* **1999**, *285* (3), 1569−1572.
(14) Li, J.; Feng, L.; Fan, L.; Zha, Y.; Guo, L.; Zhang, Q.; Chen, J.; Pang, Z.; Wang, Y.; Jiang, X.; Yang, V. C.; Wen, L. *Biomaterials* **2011**, *32* (21), 4943−4950.
(15) Kumar, P.; Wu, H.; McBride, J. L.; Jung, K.-E.; Kim, M. H.; Davidson, B. L.; Lee, S. K.; Shankar, P.; Manjunath, N. *Nature* **2007**, *448*, 39−43.

(16) Yan, H.; Wang, L.; Wang, J.; Weng, X.; Lei, H.; Wang, X.; Jiang, L.; Zhu, J.; Lu, W.; Wei, X.; Li, C. *ACS Nano* **2012**, *6*, 410−420.
(17) Koffie, R. M.; Farrar, C. T.; Saidi, L-J.; William, C. M.; Hyman, B. T.; Spires-Jones, T. L. *Proc. Natl. Acac. Sci.* **2011**, *108*, 18837−18842.
(18) Veiseh, O.; Sun, C.; Fang, C.; Bhattarai, N.; Gunn, J.; Kievit, F.; Du, K.; Pullar, B.; Lee, D.; Ellenbogen, R. G.; Olson, J.; Zhang, M. *Cancer Res.* **2009**, *69*, 6200−6207.
(19) Hwang, D. W.; Ko, H. Y.; Kim, S.-K.; Kim, D.; Lee, D. S.; Kim, S. *Chem.—Eur. J.* **2009**, *15*, 9387−9393.
(20) Guerrero, S.; Araya, E.; Fiedler, J. L.; Arias, J. I.; Adura, C.; Albericio, F.; Giralt, E.; Arias, J. L.; Fernández, M. S.; Kogan, M. J. *Nanomedicine* **2010**, *5* (6), 897−913.
(21) Guerrero, S.; Herance, J. R.; Rojas, S.; Mena, J. F.; Gispert, J. D.; Acosta, G. A.; Albericio, F.; Kogan, M. J. *Bioconjugate Chem.* **2012**, *23*, 399−408.
(22) Yim, Y. S.; Choi, J.-s.; Kim, G. T.; Kim, C. H.; Shin, T.-H.; Kim, D. G.; Cheon, J. *Chem. Commun.* **2012**, *48*, 61−63.
(23) Qiao, R.; Jia, Q.; Hüvel, S.; Xia, R.; Liu, T.; Gao, F.; Galla, H.-J.; Gao, M. *ACS Nano* **2012**, *6*, 3304−3310.
(24) Rana, S.; Bajaj, A.; Mout, R.; Rotello, V. M. *Adv. Drug Delivery Rev.* **2012**, *64*, 200−216.
(25) García, I.; Marradi, M.; Penadés, S. *Nanomedicine* **2010**, *5*, 777−792.
(26) Marradi, M.; Chiodo, F.; García, I.; Penadés, S. *Chem. Soc. Rev.* **2013**, *42*, 4728−4745.
(27) Reichardt, N. C.; Martín-Lomas, M.; Penadés, S. *Chem Soc. Rev.* **2013**, *42*, 4358−4376.
(28) (a) Prime, K. L.; Whitesides, G. M. *Science* **1991**, *252*, 1164−1167. (b) Fyrner, T.; Lee, H. H.; Mangone, A.; Ekblad, T.; Pettitt, M. E.; Callow, M. E.; Conlan, S. L.; Mutton, R.; Clare, A. S.; Konradsson, P.; Liedberg, B.; Ederth, T. *Langmuir* **2011**, *27*, 15034−15047.
(29) Van Rooy, I.; Cakir-Tascioglu, S.; Hennink, W. E.; Storm, G.; Schiffelers, R. M.; Mastrobattista, R. *Pharm. Res.* **2011**, *28*, 456−471.
(30) Nicolazzo, J. A.; Charman, S. A.; Charman, W. N. *J. Pharm. Pharmacol.* **2006**, *58*, 281−293.
(31) Bilsky, E. J.; Egleton, R. D.; Mitchell, S. A.; Palian, M. M.; Davis, P.; Huber, J. D.; Jones, H.; Yamamura, H. I.; Janders, J.; Davis, T. P.; Porreca, F.; Hruby, V. J.; Polt, R. *J. Med. Chem.* **2000**, *43*, 2586−2590.
(32) Polt, R.; Porreca, F.; Szabo, L. Z.; Bilsky, E. J.; Davis, P.; Abbruscato, T. J.; Davis, T. P.; Harvath, R.; Yamamura, H. I.; Hruby, V. J. *Proc. Natl. Acac. Sci. U.S.A.* **1994**, *91* (15), 7114−7118.
(33) Witt, K. A.; Davis, T. P. *AAPS J.* **2006**, *8*, E76−E88.
(34) Szeto, H. H.; Lovelace, J. L.; Fridland, G.; Soong, Y.; Fasolo, J.; Wu, D.; Desiderio, D. M.; Schiller, P. W. *J. Pharmacol. Exp. Ther.* **2001**, *298*, 57−61.
(35) Riss, P. J.; Kroll, C.; Nagel, V.; Rösch, F. *Bioorg. Med. Chem. Lett.* **2008**, *18*, 5364−5367.
(36) Cartier, R.; Kaufner, L.; Paulke, B. R.; Wustneck, R.; Pietschmann, S.; Michel, R.; Bruhn, H.; Pison, U. *Nanotechnology* **2007**, *18*, 195102−195114.
(37) Kim, J. S.; Kim, Y. H.; Kim, J. H.; Kang, K. W.; Tae, E. L.; Youn, H.; Kim, D.; Kim, S- K.; Kwon, J.-T.; Cho, M.-H.; Lee, Y.-S.; Jeong, J. M.; Chung, J-H; Lee, D. S. *Nanomedicine* **2012**, *7* (2), 219−229.
(38) Lee, Y.-K.; J, M. J.; Hoigebazar, L.; Yang Bo, Y.; Lee, Y.-S.; Lee, B. C.; Youn, H.; Lee, D. Soo.; Chung, J-K; Lee, M. C. *J. Nucl. Med.* **2012**, *53*, 1462−1470.
(39) Locatelli, E.; Gil, L.; Israel, L. L.; Passoni, L.; Naddaka, M.; Pucci, A.; Reese, T.; Gomez-Vallejo, V.; Milani, P.; Matteoli, M.; Llop, J.; Lellouche, J. P.; Franchini, M. C. *Int. J. Nanomed.* **2012**, *7*, 6021−6033.
(40) Clark, E. T.; Martell, A. E. *Inorg. Chim. Acta* **1991**, *181*, 273−280.
(41) Martínez-Ávila, O.; Hijazi, K.; Marradi, M.; Clavel, C.; Campion, C.; Kelly, C.; Penadés, S. *Chem.—Eur. J.* **2009**, *15*, 9874−9888.
(42) Barrientos, A. G.; de la Fuente, J. M.; Rojas, T. C.; Fernández, A.; Penadés, S. *Chem.—Eur. J.* **2003**, *9*, 1909−1921.
(43) Costantino, L.; Gandolfi, F.; Tosi, G.; Rivasi, F.; Vandelli, M. A.; Forni, F. *J. Controlled Release* **2005**, *108*, 84−96.

456

dx.doi.org/10.1021/ja411096m | *J. Am. Chem. Soc.* 2014, 136, 449−457

(44) Tosi, G.; Fano, R. A.; Bondioli, L.; Badiali, L.; Benassi, R.; Rivasi, F.; Ruozi, B.; Forni, F.; Vandelli, M. A. *Nanomedicine* **2011**, *6* (3), 423−436.

(45) Pert, C. B.; Pert, A.; Chang, J. K.; Fong, B. T. W. *Science* **1976**, *194*, 330−332.

(46) Vogel, Z.; Alstein, M. *Prog. Biochem. Pharmocol.* **1980**, *16*, 49−59.

(47) Barrientos, A. G.; de la Fuente, J. M.; Jiménez, M.; Solís, D.; Cañada, D.; Martín-Lomas, M.; Penadés, S. *Carbohydr. Res.* **2009**, *344*, 1474−1478.

(48) Hostetler, M. J.; Templeton, A. C.; Murray, R. W. *Langmuir* **1999**, *15*, 3782−3789.

(49) Velikyan, I.; Maecke, H.; Langstrom, B. *Bioconjugate Chem.* **2008**, *19*, 569−573.

(50) Slack, J. D.; Kanke, M.; Simmons, G. H; DeLuca, P. P. *J. Pharm. Sci.* **1981**, *6*, 660−664.

(51) (a) Litzinger, D. C.; Buiting, A. M.; van Rooijen, N.; Huang, L. *Biochim. Biophys. Acta* **1994**, *1190* (1), 99−107. (b) Herant, M.; Heinrich, V.; Dembo, M. *J. Cell. Sci.* **2006**, *119*, 1903−1913.

(52) Pérez-Campaña, C.; Gómez-Vallejo, V.; Puigivila, M.; Martin, A.; Calvo-Fernández, T.; Moya, S. E.; Ziolo, R. F.; Reese, T.; Llop, J. *ACS Nano* **2013**, *7* (4), 3498−3505.

(53) Sun, G.; Hagooly, A.; Xu, J.; Nystrom, A. M.; Li, Z.; Rossin, R.; Moore, D. A.; Wooley, K. L.; Welch, M. J. *Biomacromolecules* **2008**, *9*, 1997−2006.

(54) Semmler-Behnke, M.; Kreyling, W. G.; Lipka, J.; Fertsch, S.; Wenk, A.; Takenaka, S.; Schmid, G.; Brandau, W. *Small* **2008**, *4* (12), 2108−2111.

(55) (a) De Jong, W. H.; Hagens, W. I.; Krystek, P.; Burger, M. C.; Sips, A. J. A. M.; Geertsma, R. E. *Biomaterials* **2008**, *29*, 1912−1919. (b) Sonavanea, G.; Tomodaa, K.; Makino, K. *Colloids Surf., B* **2008**, *66*, 274−280. (c) Lasagna-Reeves, C.; Gonzalez-Romero, D.; Barria, M. A.; Olmedo, I.; Clos, A.; Sadagopa Ramanujam, V. M.; Urayama, A.; Vergara, L.; Kogan, M. J.; Soto, C. *Biochem. Biophys. Res. Commun.* **2010**, *393*, 649−655.

(56) Sá, A. D.; Prata, M. I. M.; Geraldes, C. F. G. C.; André, J. P. *J. Inorg. Biochem.* **2010**, *104*, 1051−1062.

(57) Khlebtsov, N.; Dykman, L. *Chem. Soc. Rev.* **2011**, *40*, 1647−1671.

(58) Longmire, M.; Choyke, P L.; Kobayashi, H. *Nanomedicine* **2008**, *3*, 703−717.

(59) Gref, R.; Minamitake, Y.; Peracchia, M. T.; Trubetskoy, V.; Torchilin, V.; Langer, R. *Science* **1994**, *263*, 1600−1603.

(60) Lockman, P. R.; Oyewumi, M. O.; Koziara, J. M.; Roder, K. E.; Mumper, R. J.; Allen, D. D. *J. Controlled Release* **2003**, *93* (3), 271−282.

(61) Xie, Y.; Ye, L.; Zhang, X.; Cui, W.; Lou, J.; Nagai, T.; Hou, X. *J. Controlled Release* **2005**, *105* (1−2), 106−119.

(62) Ke, W.; Shao, K.; Huang, R.; Han, L.; Liu, Y.; Li, J.; Kuang, Y.; Ye, L.; Lou, J.; Jiang, C. *Biomaterials* **2009**, *30* (36), 6976−6985.

(63) Hostetler, M. J.; Wingate, J. E.; Zhong, C.-J.; Harris, J. E.; Vachet, R. W.; Clark, M. R.; Londono, J. D.; Green, S. J.; Stokes, J. J.; Wignall, G. D.; Glish, G. L.; Porter, M. D.; Evans, N. D.; Murray, R. W. *Langmuir* **1998**, *14*, 17−30.